

Wigner function for a driven anharmonic oscillator

K V Kheruntsyan

Department of Physics, University of Queensland, St Lucia, QLD 4072, Australia

Received 3 September 1998, in final form 23 November 1998

Abstract. We consider the quantum model of a driven anharmonic oscillator, in the presence of dissipation, and present an exact analytic solution for the corresponding Wigner function in the steady-state regime. This provides explicit phase-space images of the resulting state of the cavity mode, and allows us to understand how the quantum interference is built up into it. The photon number probability distribution is calculated and analysed as well. We monitor the transition from the semiclassical to extreme quantum regime of operation, and identify qualitative changes, where the conventional characteristics of the model, such as bistability or turning points, become meaningless.

Keywords: Quantum quasiprobabilities, Wigner function, photon statistics, anharmonic oscillator, dissipative, nonlinear quantum noise effects

1. Introduction

Recent developments in quantum optics have resulted in significantly increased interest in the Wigner function [1]. Being a joint quasiprobability distribution for the position and momentum observables, the Wigner function has a one-to-one correspondence to the density matrix, thus providing complete information about a given quantum system. It also allows us to visualize the quantum dynamical image of a quantum state in the phase space—an important problem since the early stages of quantum mechanics. As compared with other quasiprobability distributions, the Wigner function has the advantage of best describing nonclassical states of light in quantum optics, including the quantum superposition and interference phenomena (see, e.g., [2] and references therein). Most significantly, the Wigner function has been shown to be experimentally reconstructible, by a measurement of a set of probability distributions of the light quadrature-phase amplitudes, using the method of quantum tomography [3–5]. These quadrature probabilities are simply the marginal distributions of the Wigner function.

A number of model Hamiltonians and particular idealized nonclassical states of light has been successfully described with use of the Wigner function. However, very few realistic quantum optical systems that include dissipation, and lead to generation of nonclassical light, are known to be analysed in terms of the Wigner function. This is especially true, if we look for exact analytic results. The difficulty here is that nonlinear optical interactions usually generate unsolvable Fokker–Planck-type equations for the Wigner function, that contain third- or higher-order derivative terms. To stress the importance of incorporating the dissipation effects into the idealized models and underlying nonclassical states, we only mention the crucial sensitivity of the famous Schrödinger-cat states to losses.

An example of a quantum optical dissipative model that has been analysed in terms of the Wigner function is the well known parametric oscillator (PO) model. An approximate result for the corresponding Wigner function, based on the solution of the truncated Fokker–Planck equation, has been given in [6]. Another approach, based on the relation of the Wigner function to the known solution of the Fokker–Planck equation in positive P -representation, has been used in [7] to analyse quantum superposition and interference effects in PO. This approach has been further developed in [8], to utilize a complex P -representation solution for a generalized model of PO, thus allowing one to obtain a simple analytic result for the corresponding Wigner function. Numerical techniques to analyse the Wigner function for the PO subjected to both one- and two-photon loss mechanisms, and recently for the model of three-photon down-conversion, have also been used [9,25]. In addition, we mention a recent paper [10] which provides a novel approach for the direct computation of the Wigner function from phase space.

In this paper we present a new Wigner-function solution for a dissipative quantum mechanical system. We consider the well known model of a driven anharmonic oscillator (AHO), and derive an exact analytic result for the corresponding Wigner function in the steady state.

The AHO is one of the most fundamental models in quantum optics [11–17]. It describes a self-interaction (self-phase modulation or Kerr interaction) of a mode of radiation field in a cavity filled by a $\chi^{(3)}$ -nonlinear medium. The model is known to be responsible, in particular, for dispersive optical bistability and for amplitude squeezing, and has also been used to describe formation of Schrödinger-cat states. The effective interaction Hamiltonian of the AHO model has also a relevance in description of Bose–Einstein condensates, in a simple single-mode approximation [18].

With dissipation included, the driven AHO model has been solved exactly in the steady-state regime, in terms of the Fokker–Planck equation in complex P -representation [11]. Using this solution we derive here an exact and surprisingly simple analytic result for the corresponding Wigner function. This provides explicit phase-space images of the steady state of the system and of the underlying nonclassical effects.

Since our results are based on the exact nonlinear treatment of quantum fluctuations, it is particularly interesting to focus on the extreme quantum regime of operation, corresponding to extremely high nonlinearities or low dissipation. This brings out a rather rich variety of phase transition images in the bistable operation regime, qualitatively different to what one would expect from the corresponding semiclassical analysis. We also calculate the photon number probability distribution function which provides a better insight to the qualitative changes in the transition from the semiclassical to the extreme quantum regime.

2. Hamiltonian and exact quantum (quasi)probabilities

The anharmonic oscillator model we consider describes a single intracavity mode which is driven by an external coherent field and which undergoes the process of self-phase modulation (Kerr interaction) in a $\chi^{(3)}$ -nonlinear medium. We allow for usual one-photon losses for the cavity mode, and, in addition, incorporate a two-photon absorption. This nonlinear system can be modelled, in the rotating wave approximation, by the following Hamiltonian [11, 19]:

$$H = \hbar\omega_c a^\dagger a + \hbar\chi'' a^{\dagger 2} a^2 + i\hbar(Ee^{-i\omega_L t} a^\dagger - E^* e^{i\omega_L t} a) + a^\dagger \Gamma_1^\dagger + a^\dagger \Gamma_1 + a^2 \Gamma_2^\dagger + a^{\dagger 2} \Gamma_2. \quad (1)$$

Here a^\dagger (a) is the creation (annihilation) operator for the cavity mode with the frequency ω_c , χ'' is the nonlinear coupling constant for the self-phase modulation process, proportional to the third-order susceptibility $\chi^{(3)}$, E is the amplitude of the coherent driving field with the frequency ω_L . In addition, Γ_1 , Γ_1^\dagger and Γ_2 , Γ_2^\dagger are reservoir operators describing one-photon and two-photon losses, which will give rise to the damping rates γ and χ' , respectively.

Utilizing standard techniques (see, e.g., [20, 21]) to eliminate the reservoir operators, one may obtain the following interaction picture master equation for the density matrix ρ of the cavity mode:

$$\begin{aligned} \frac{\partial \rho}{\partial t} = & -i\Delta[a^\dagger a, \rho] - i\chi''[a^{\dagger 2} a^2, \rho] + [Ea^\dagger - E^* a, \rho] \\ & + \gamma(2a\rho a^\dagger - \rho a^\dagger a - a^\dagger a\rho) \\ & + \chi'(2a^2 \rho a^{\dagger 2} - \rho a^{\dagger 2} a^2 - a^{\dagger 2} a^2 \rho), \end{aligned} \quad (2)$$

where $\Delta = \omega_c - \omega_L$ is the cavity detuning. The master equation is then transformed into a Fokker–Planck equation. We follow here the approach of [11], utilizing the complex P -representation of the density matrix. The resulting Fokker–Planck equation for the quasiprobability distribution function $P(\alpha, \alpha^\dagger)$ has the following form:

$$\frac{\partial P(\alpha, \alpha^\dagger)}{\partial t} = \left\{ \frac{\partial}{\partial \alpha} (\bar{\gamma} \alpha + 2\chi \alpha^2 \alpha^\dagger - E) \right.$$

$$\left. + \frac{\partial}{\partial \alpha^\dagger} (\bar{\gamma}^* \alpha^\dagger + 2\chi^* \alpha^{\dagger 2} \alpha - E^*) + \frac{1}{2} \frac{\partial^2}{\partial \alpha^2} (-2\chi \alpha^2) + \frac{1}{2} \frac{\partial^2}{\partial \alpha^{\dagger 2}} (-2\chi^* \alpha^{\dagger 2}) \right\} P(\alpha, \alpha^\dagger), \quad (3)$$

where $\bar{\gamma}$ and χ are defined as follows: $\bar{\gamma} = \gamma + i\Delta$, $\chi = \chi' + i\chi''$. We note that in the complex P -representation the amplitudes α, α^\dagger are independent complex c -number variables corresponding to the operators a, a^\dagger , and their integration domains are to be chosen as contour integrals in the individual complex planes. The Fokker–Planck equation (3) can be solved exactly, in the steady-state regime, using the method of potential equations. This results in the following form of steady-state P -function [11]:

$$P_s(\alpha, \alpha^\dagger) = \mathcal{N} \alpha^{\lambda-2} (\alpha^\dagger)^{\lambda^*-2} \exp\left(\frac{\varepsilon}{\alpha} + \frac{\varepsilon^*}{\alpha^\dagger} + 2\alpha\alpha^\dagger\right), \quad (4)$$

where \mathcal{N} is the normalization constant, and we have introduced the following parameters:

$$\varepsilon = \frac{E}{\chi}, \quad \lambda = \frac{\bar{\gamma}}{\chi}. \quad (5)$$

The steady-state solution (4) has been used in [11] to derive the normally ordered operator moments $\langle a^{\dagger m} a^m \rangle$, yielding at:

$$\langle a^{\dagger m} a^m \rangle = \frac{|\varepsilon|^{2m} \Gamma(\lambda) \Gamma(\lambda^*) {}_0F_2(m + \lambda, m + \lambda^*, 2|\varepsilon|^2)}{\Gamma(m + \lambda) \Gamma(m + \lambda^*) {}_0F_2(\lambda, \lambda^*, 2|\varepsilon|^2)}, \quad (6)$$

where ${}_0F_2(a, b, z)$ is a hypergeometric function

$${}_0F_2(a, b, z) = \sum_{k=0}^{\infty} \frac{z^k \Gamma(a) \Gamma(b)}{k! \Gamma(k+a) \Gamma(k+b)}. \quad (7)$$

Together with the semiclassical steady states, showing bistability (hysteresis) in the amplitude of the cavity mode versus the driving field amplitude, the exact quantum mechanical mean amplitude $\langle a \rangle$ and the second-order correlation function have been analysed in [11]. This was able to show the non-equilibrium nature of the phase transition in the system, and to predict nonclassical effects of reduction of photon number fluctuations and photon antibunching, within the exact nonlinear treatment of quantum fluctuations. In terms of the mode quadrature-phase amplitudes, the nonclassical photon statistics in the AHO model is manifested also as an amplitude squeezing [12].

In what follows, instead of describing the quantum statistical properties of the cavity mode via operator moments, we present an analysis in terms of quantum (quasi)probability distributions. Using the steady-state solution (4), we derive exact analytical results for the photon number probability distribution function and the Wigner function.

The photon number probability distribution $p(n) = \langle n | \rho | n \rangle$ can be expressed in terms of the complex P -representation as follows:

$$p(n) = \frac{1}{n!} \iint_C d\alpha d\alpha^\dagger \alpha^n (\alpha^\dagger)^n \exp(-\alpha\alpha^\dagger) P(\alpha, \alpha^\dagger), \quad (8)$$

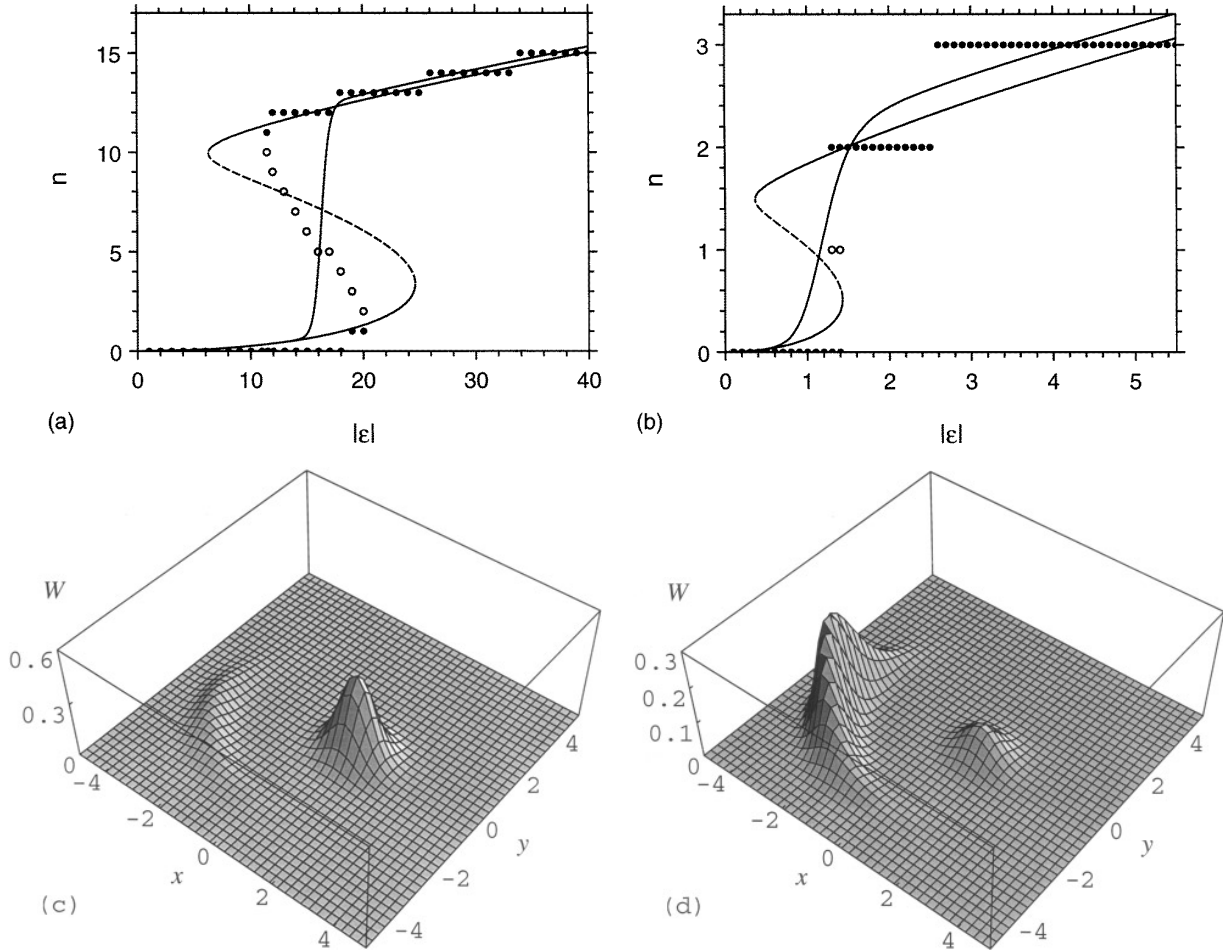


Figure 1. (a), (b) A quantum mechanical mean intensity (full curve), the semiclassical intensity (the curve with a broken part), and the locations of local maxima (full circles) and minima (empty circles) in the $p(n)$ -function as depending on $|\varepsilon|$, for: (a) $\Delta/\chi'' = -20$ and $\gamma/\chi'' = 2$; (b) $\Delta/\chi'' = -3$ and $\gamma/\chi'' = 0.3$. (c), (d) The Wigner function $W(x, y)$ for the same values of Δ/χ'' and γ/χ'' as in (a), and for: (c) $|\varepsilon| = 12$, and (d) $|\varepsilon| = 17$.

where C is an appropriate integration contour for each of the variables α and α^\dagger , in the individual complex planes. Substituting the steady-state P -function, equation (4), we then expand the resulting exponential term $\exp(-\alpha\alpha^\dagger)$, thus arriving at a separation of variables in the two integrals. Transforming next to new variables $\delta = \varepsilon/\alpha$ and $\delta^\dagger = \varepsilon^*/\alpha^\dagger$, we find that the integrals are identical to the Hankel representation of the Γ -function [22]:

$$\frac{1}{\Gamma(z)} = \frac{1}{2\pi i} \int_C dt t^{-z} e^t, \quad (9)$$

where C is the integration contour (Hankel path), which starts at $(-\infty)$ on the real axis, encircles the origin in an anticlockwise direction, and returns back to $(-\infty)$. Also taking into account the normalization [11], these give the following final result for the steady-state photon probability distribution function:

$$p(n) = \frac{|\varepsilon|^{2n} \Gamma(\lambda) \Gamma(\lambda^*)}{n! {}_0F_2(\lambda, \lambda^*, 2|\varepsilon|^2)} \times \sum_{k=0}^{\infty} \frac{|\varepsilon|^{2k}}{k! \Gamma(k+n+\lambda) \Gamma(k+n+\lambda^*)}. \quad (10)$$

The Wigner function $W(\alpha)$ is found as follows. Using a standard definition

$$W(\alpha) = \frac{2}{\pi} e^{-2|\alpha|^2} \int d^2\gamma \text{Tr}(\rho e^{\gamma\alpha^\dagger - \gamma^*a}) e^{\gamma^*\alpha - \gamma a^*}, \quad (11)$$

one can express the Wigner function in terms of the P -representation:

$$W(\alpha) = \frac{2}{\pi} e^{-2|\alpha|^2} \iint_C d\beta d\beta^\dagger P(\beta, \beta^\dagger) \times \exp(2\alpha^*\beta + 2\alpha\beta^\dagger - 2\beta\beta^\dagger). \quad (12)$$

Substituting the steady-state solution (4), we note that the mutual cancellation of the exponential terms $\exp(-2\beta\beta^\dagger)$ and $\exp(2\beta\beta^\dagger)$ directly leads to the separation of variables in the integrals. The variable change $\delta = \varepsilon/\beta$ and $\delta^\dagger = \varepsilon^*/\beta^\dagger$ allows us then to recognize an integral representation of the Bessel function [23]:

$$2\pi i J_\nu(z) = \left(\frac{z}{2}\right)^\nu \int_C dt t^{-\nu-1} \exp\left(t - \frac{z^2}{4t}\right), \quad (13)$$

where C is the same Hankel path as above.

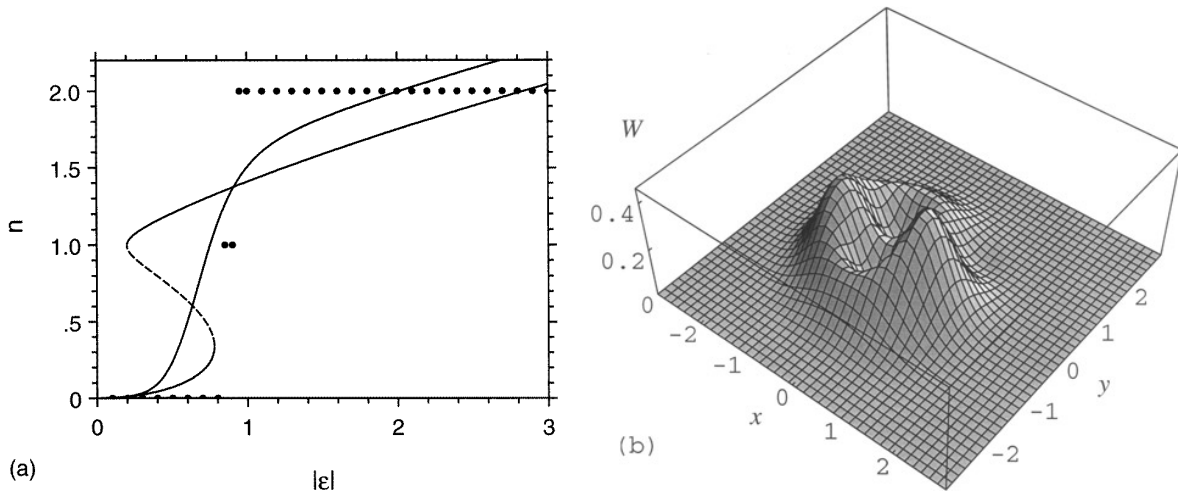


Figure 2. The same as in figure 1 but for $\Delta/\chi'' = -2$ and $\gamma/\chi'' = 0.2$; (b) $|\varepsilon| = 0.8$.

The final result for the steady-state Wigner function takes the following explicit form:

$$W(\alpha) = N e^{-2|\alpha|^2} \left| \frac{J_{\lambda-1}(\sqrt{-8\varepsilon\alpha^*})}{(\alpha^*)^{\frac{\lambda-1}{2}}} \right|^2, \quad (14)$$

where N is the normalization constant.

3. Results and discussion

In our numerical analysis of the probability distribution function $p(n)$ and the Wigner function we focus, for simplicity, on the case $\chi' = 0$, that is $\chi = i\chi''$, and therefore $\lambda = (\Delta/\chi'') - i(\gamma/\chi'')$. (The influence of a nonzero χ' is discussed at the end of this section.) In addition, we choose, without loss of generality, the phase ϕ of the driving field $E = |E| \exp(i\phi)$ equal to $\phi = -\pi/2$, so that $-\varepsilon = |\varepsilon|$.

In figures 1(a), 1(b) and 2(a)–4(a) we plot the cavity mode steady-state quantum mechanical mean intensity $n = \langle a^\dagger a \rangle$ (in photon number units; full curves), the corresponding semiclassical result [11] (the curve with a broken segment), and also the locations of the local maxima (full circles) and local minima (empty circles) in the $p(n)$ -function, as depending on $|\varepsilon|$. The graphs are given for different values of the relative detuning Δ/χ'' and the relation of the damping constant to the nonlinearity γ/χ'' . The values of Δ/χ'' and γ/χ'' are chosen to lead to bistability [11], in terms of the semiclassical steady-state solutions as depending on $|\varepsilon|$. This requires that $(\Delta/\gamma)^2 > 3$ and $\Delta/\chi'' < 0$; the broken segments of the semiclassical curves correspond to the unstable solution, while the full parts correspond to the lower and upper branches of the stable solutions.

The monotonic increase (no hysteresis) of the quantum mechanical mean intensity, which includes quantum fluctuations, is a usual consequence of quantum statistical averaging. The presence or absence of bistability, within the exact quantum statistical treatment, can still be revealed by analysing the photon number distribution function $p(n)$ for different values of $|\varepsilon|$. In this case the bistability is manifested in the coexistence of two local maxima in $p(n)$. For relatively small nonlinearities and strong damping

($\gamma/\chi'' \gg 1$), when the usual linearized treatment of quantum fluctuations around the stable semiclassical steady states is valid, the locations of the maxima coincide with the stable branches of the semiclassical intensity. The minimum in $p(n)$, located between the two maxima, corresponds to the unstable semiclassical solution.

With decrease in the relation γ/χ'' , the nonlinear effects of quantum fluctuations become essential (the linearization starts to fail), and as a consequence the locations of the maxima/minima in the $p(n)$ -function depart from the semiclassical curve. This is already seen in the example of figure 1(a), while further shifts of the curves, corresponding to entering into an extreme quantum regime of operation (smaller γ/χ''), are represented in figures 1(b) and 2(a)–4(a). As we see, the shifts between the quantum and semiclassical curves are not simply of a quantitative character. In the extreme quantum regime we observe (figures 2(a)–4(a)) qualitative changes, so that the bistability (in semiclassical terms) does not now manifest itself through the structure of the $p(n)$ -function, as it only has one maximum. In other words this implies that the term bistability (and, correspondingly, the associated turning points or threshold) becomes meaningless in this regime. Instead, the most probable values of n versus $|\varepsilon|$ are simply represented as a sequence of relatively wide plateaux.

While the analysis of the photon number probability distribution provides rather detailed understanding of the nonlinear dynamics of the system, this still is incomplete since the $p(n)$ -function is a phase-insensitive quantity. Instead, a complete phase-space quantum statistical treatment of our model can be achieved via the Wigner function given by equation (14).

Examples of the Wigner function $W(\alpha) = W(x, y)$, where $x = \text{Re } \alpha$ and $y = \text{Im } \alpha$, are given in figures 1–4, for the same values of the parameters Δ/χ'' and γ/χ'' as in the corresponding graphs (a). Different plots of the Wigner function correspond to different values of $|\varepsilon|$, chosen to monitor the bistability region or the transition from the lower to the upper level of excitation. The graphs in figure 1 are far from representing the extreme quantum regime, and we see expected images of rather adequate correspondence

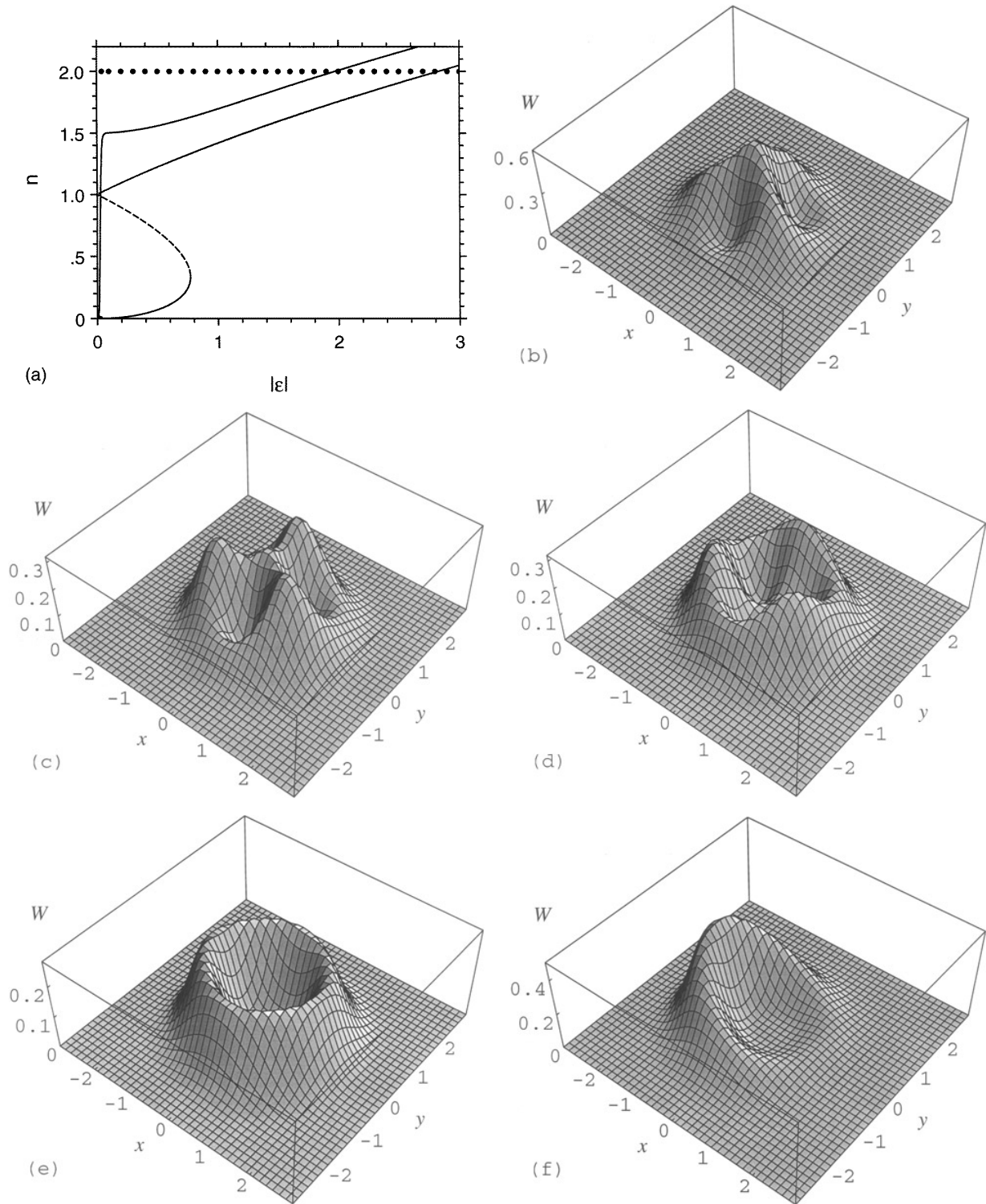


Figure 3. The same as in figure 1 but for $\Delta/\chi'' = -2$ and $\gamma/\chi'' = 10^{-5}$; (b) $|\varepsilon| = 0.025$, (c) $|\varepsilon| = 0.03$, (d) $|\varepsilon| = 0.04$, (e) $|\varepsilon| = 0.08$, and (f) $|\varepsilon| = 1$.

to the semiclassical steady states. The radial (amplitude) squeezing of the upper branch, which represents the known property of the AHO model to produce quadrature amplitude or photon number squeezing [11, 12, 16], is also clearly seen in the figures.

The graph of figure 2(b) is given for a smaller value of γ/χ'' , corresponding to entering into an extreme quantum

regime of operation. The value of Δ/χ'' is chosen so that the relation between Δ/χ'' and γ/χ'' is kept the same as in figure 1, leading to the same shape (except for a scaling factor) of the semiclassical intensity curves. We see here that the two coexisting humps in the Wigner function are overlapping, and an additional complicated structure becomes prominent.

The most dramatic change in the scenario of the

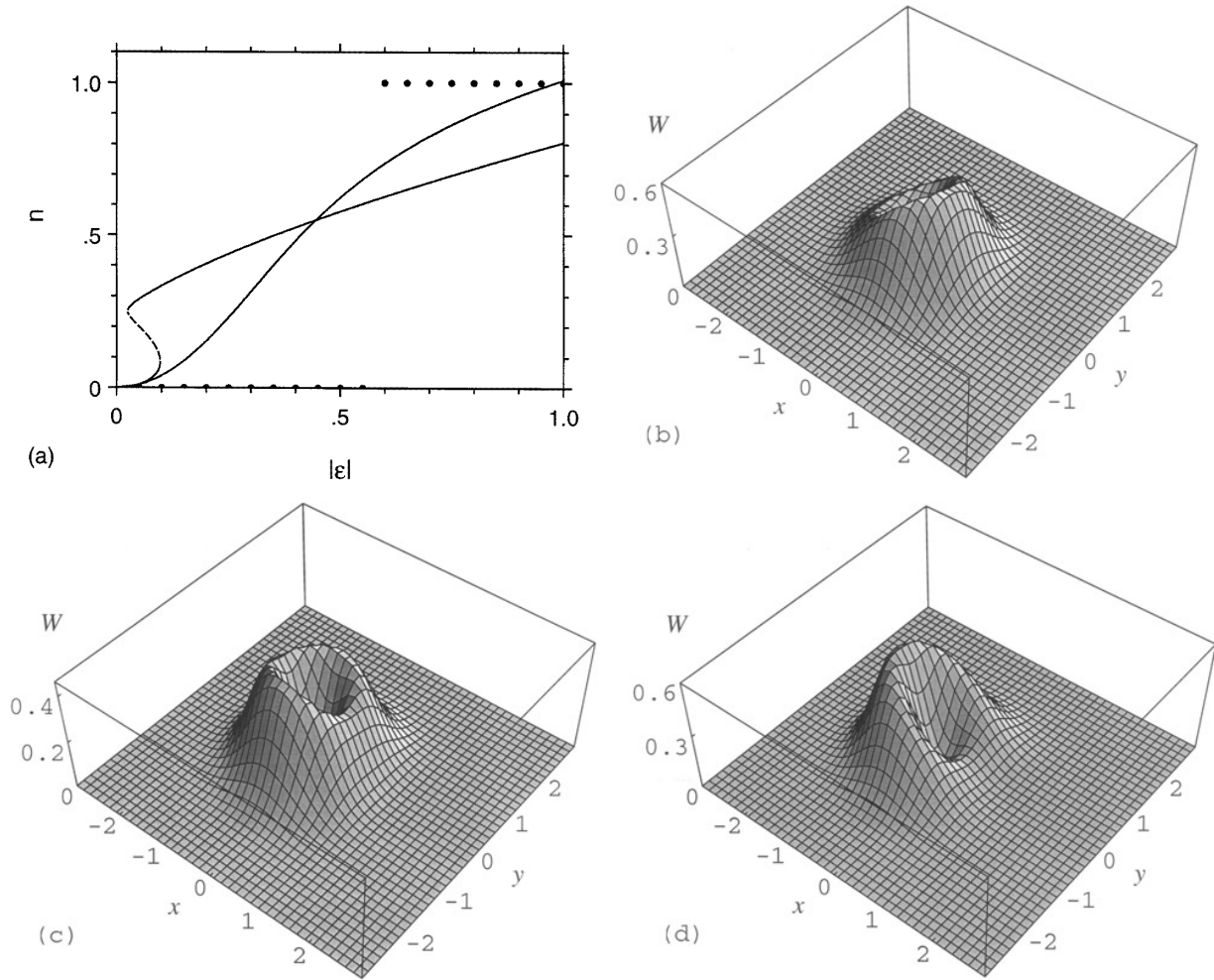


Figure 4. The same as in figure 1 but for $\Delta/\chi'' = -0.5$ and $\gamma/\chi'' = 0.05$; (b) $|\varepsilon| = 0.4$, (c) $|\varepsilon| = 0.55$, and (d) $|\varepsilon| = 0.8$.

transition from the lower to the upper level of excitation, in the extreme quantum regime, is represented in the phase-space images of figures 3(b)–(f) and 4(b)–(d). In figure 4 the relation between Δ/χ'' and γ/χ'' is chosen as in the cases of figures 1 and 2, while in figure 3 we choose γ/χ'' much smaller. The structure of the Wigner function contains now oscillating features and may show more than two local maxima and minima which clearly cannot be identified with the semiclassical steady states.

Noticing the complicated structure and oscillating features in the Wigner function, it is natural to treat these within the context of quantum superposition and interference phenomena. The quantum superposition, in the case of pure states, is known to lead to manifestly oscillating behaviour of the Wigner function, with interference fringes being spread even into negative-valued regions [2]. Regarding to this point we emphasize, however, that one of the main properties of our result for the Wigner function, is that it is positive everywhere. In addition, due to the presence of dissipation it corresponds to a statistical mixture. Nevertheless, quantum superposition and interference effects are still relevant here. The simplest argument is that the effective quartic interaction Hamiltonian in equation (1) is known to have photon number eigenstates, and also to produce, in the case of evolution from an initial

coherent state, superposition of coherent states (Schrödinger cats). In both these cases the Wigner function has manifestly oscillating behaviour and negative-valued regions [2]. With the dissipation included, the interference effects in the AHO model evolving from the initial coherent state have been analysed in [17], in terms of the Q -function dynamics.

Returning to our model, it is natural to expect that these quantum coherences contribute in the resulting mixture state, even if we do not specify what kind of mixture of what kind of superposition states we end up with. We note here that an exact analytic expression for the steady-state density matrix ρ of the cavity mode, in the Fock states basis, can be obtained using the above complex P -solution and the contour integration technique, yielding at:

$$\rho = \frac{\Gamma(\lambda)\Gamma(\lambda^*)}{{}_0F_2(\lambda, \lambda^*, 2|\varepsilon|^2)} \times \sum_{n,m} \frac{(\varepsilon)^n (\varepsilon^*)^m}{\sqrt{n!}\sqrt{m!}} \frac{{}_0F_2(\lambda+n, \lambda^*+m, |\varepsilon|^2)}{\Gamma(\lambda+n)\Gamma(\lambda^*+m)} |n\rangle\langle m|, \quad (15)$$

but this is more difficult to analyse than the Wigner function, equation (14).

To examine the manifestation of the quantum interference in our Wigner function, we firstly consider for simplicity the limit $\gamma/\chi'' \rightarrow 0$ and $\Delta/\chi'' = \frac{1}{2}$. In this

case $\lambda = \frac{1}{2}$, and the Bessel function in equation (14) can be expressed in terms of elementary functions [23]: $J_{-1/2} = \sqrt{2/(\pi z)} \cos z$. This gives:

$$W(x, y)|_{\lambda=1/2} = \frac{N}{\pi \sqrt{2|\varepsilon|}} e^{-2(x^2+y^2)} \left| \cos \left(\sqrt{8|\varepsilon|(x+iy)} \right) \right|^2. \quad (16)$$

The x -dependence of the Wigner function, in the region $x > 0$, is simply given by: $W(x, y = 0) \propto \exp(-2x^2) \cos^2(\sqrt{8|\varepsilon|x})$. This clearly demonstrates the character of oscillations in the Wigner function. For negative valued x we have: $W(x, y = 0) \propto \exp(-2x^2) [\exp(\sqrt{8|\varepsilon||x|}) + \exp(-\sqrt{8|\varepsilon||x|})]^2$, which is a single peaked function, with the maximum value being much greater than the values in the region $x > 0$. With the dissipation included, a phase-space image of oscillations in the Wigner function is given in figure 5(a). The characteristic amplitude of the oscillations is, however, small compared with the main contribution located in the region $x < 0$, so that the fringes are not seen in the entire domain of x (figure 5(b)).

More information on the structure of our Wigner function can be gained by considering a set of integer values of Δ/χ'' , together with the limit $\gamma/\chi'' \rightarrow 0$. This case results in integer values of λ ($\lambda \equiv m = 0, \pm 1, \pm 2, \dots$), with the x -dependence of the Wigner function being given by:

$$W(x, y = 0)|_{\lambda=m} = N e^{-2x^2} |x|^{m-1} \left| J_m \left(\sqrt{8|\varepsilon|x} \right) \right|^2. \quad (17)$$

Here the cases with $m < 0$ are treated using the property that $J_{-m}(x) = (-1)^m J_m(x)$. For $x < 0$ the Bessel function $J_m(\sqrt{8|\varepsilon|x})$ is transformed into the modified Bessel function of the first kind $I_m(\sqrt{8|\varepsilon||x|})$ through the relation $J_m(ix) = i^m I_m(x)$. The function $I_m(x)$ is known to be monotonically increasing, so that together with the factors e^{-2x^2} and $|x|^{m-1}$ this results in a single-peaked shape of the resulting Wigner function $W(x, y = 0)$ for $x < 0$. The oscillating structure in the $W(x, y = 0)$ -function occurs in the region $x > 0$, due to the well known oscillating properties of the Bessel function $J_m(x)$ and hence of $|J_m(\sqrt{8|\varepsilon|x})|^2$. The oscillations are of aperiodic (with an increasing 'period') character due to the square root dependence on x , and have decreasing amplitudes. The distances between the oscillation peaks also depend on $|\varepsilon|$, and all these are modulated by the factor $e^{-2x^2} |x|^{m-1}$. This modulation curve has a single peak, for $m > 1$, located at $\sqrt{m-1}/2$, or is monotonically decreasing for $m \leq 0$. In either case this strongly suppresses oscillations at large x , however the modulation peak (in the case $m > 1$) may also have a 'resonantly' enhancing influence on the interference fringes that are within the width of the peak.

All these features build up into a variety of resulting shapes of the modulated oscillations, the overall visibility of which, in the entire domain of x , will depend on the relative weights of the contributions in the $x < 0$ and $x > 0$ regions. A general conclusion is that the structure of the $W(x, y)$ -function may contain either only few visible fringes (peaks), or several interference fringes which are however invisible on the scale of the leading peak.

Let us focus now on the characteristic values of parameters and the relevance of our results to physically accessible regimes. Considering, for example, a high- Q cavity with $\gamma \sim 10^6 \text{ s}^{-1}$ and conventional values

of cubic nonlinearities in atomic gases would lead to the relation $\gamma/\chi'' \sim 10^7-10^8$. These are typical values to employ successfully a semiclassical analysis and linearized treatment of quantum fluctuation. Correspondingly, the most interesting and nontrivial effects studied here for the extreme quantum regime ($\gamma/\chi'' \leq 1$) are far from being observable, in this case.

However, a recent analysis [24] suggests a new scheme for the AHO model, which utilizes atomic dark resonances and allows to achieve giant optical nonlinearities. According to this proposal such a scheme can decrease the relation γ/χ'' by several orders of magnitude, leading to $\gamma/\chi'' \sim 0.05$. In terms of our results for the intracavity photon number probabilities and the Wigner function, this particular regime, studied in [24] for the case of zero cavity detuning, is represented in figure 6.

The concept of the so-called photon blockade, introduced in [24], can easily be interpreted and seen here via the dynamics of the most probable n -values in the $p(n)$ -function, as depending on $|\varepsilon|$ (circles in figure 6(a)): despite the increase of $|\varepsilon|$ over a relatively wide domain, the injection of an additional photon into the cavity is blocked. It should be also noted here that the parameter $|\varepsilon| = |E|/\chi''$ can be expressed in terms of the cavity input fields as follows. Since $|E| = \sqrt{2\gamma} |a_{in}|$, where a_{in} is an annihilation operator for the coherent driving field at the input of the cavity (so that $\langle a_{in}^\dagger a_{in} \rangle = |a_{in}|^2 \equiv f_{in}$ represents the photon flux or average number of photons per unit time), then we obtain that $|\varepsilon|^2 = 2\gamma f_{in}/(\chi'')^2$. This can also be rewritten in terms of the relation γ/χ'' and γ as follows: $f_{in} = \gamma |\varepsilon|^2 (\gamma/\chi'')^{-2}/2$, implying that for $|\varepsilon| \sim 1$ and the above-mentioned values of $\gamma \sim 10^6 \text{ s}^{-1}$ and $\gamma/\chi'' \sim 0.05$, the corresponding cavity input photon flux is $f_{in} \sim 2 \times 10^8$ photons per second.

Finally, let us discuss the influence of the two-photon loss or absorption mechanism which is incorporated in our general results through the damping rate χ' , the real part of the coefficient $\chi = \chi' + i\chi''$. Mathematically, complex values of χ allowed us to treat both the effects of the Kerr nonlinearity (χ'') and two-photon absorption (χ') within a unified theory. In practical terms, this can be applied to physically different nonlinear systems, where the intracavity medium has a third-order polarizability (then $\chi = i\chi''$), or is a two-photon absorber ($\chi = \chi'$), or else one may even consider a combination of these two types of nonlinearity within a single cavity ($\chi = \chi' + i\chi''$). (In each case, the one-photon damping constant γ is due to losses through the input-output mirror of the cavity.)

In the discussion and examples given above, the two-photon absorption coefficient was set to zero, for the sake of simplicity. Once, however, the characteristic behaviour of the system in different operation regimes is revealed, then it can be easily generalized to the cases with nonzero χ' . This is simply seen from the fact that the actual parameters that govern the behaviour of the system (and have been used in the analyses) are $\text{Re } \lambda$, $\text{Im } \lambda$, and $|\varepsilon|$ (see equation (5)):

$$\text{Re } \lambda = \frac{\gamma \chi' + \Delta \chi''}{(\chi')^2 + (\chi'')^2}, \quad (18)$$

$$\text{Im } \lambda = \frac{\Delta \chi' - \gamma \chi''}{(\chi')^2 + (\chi'')^2}, \quad (19)$$

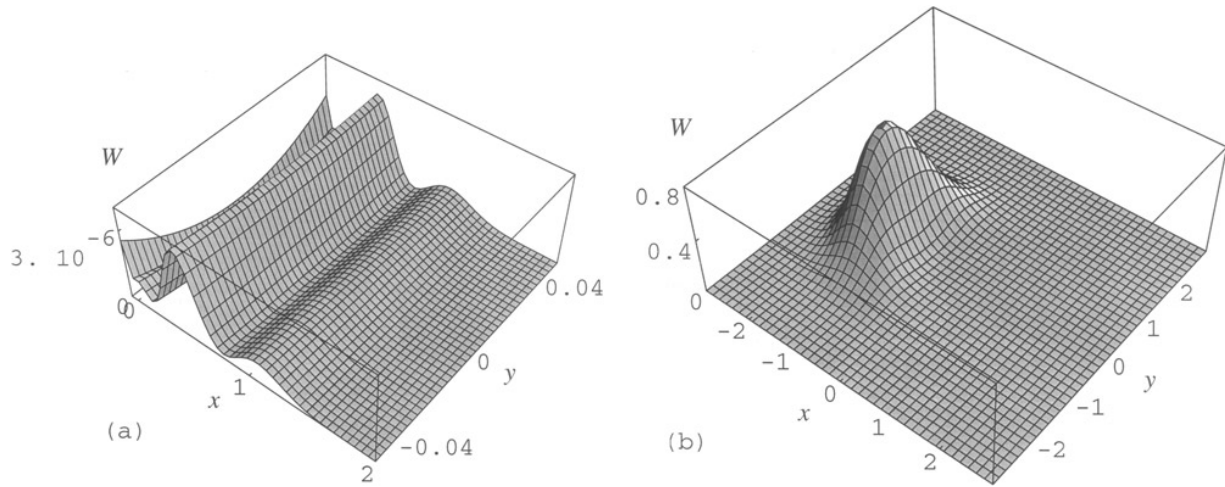


Figure 5. Wigner function $W(x, y)$ for $\Delta/\chi'' = 0.5$, $\gamma/\chi'' = 0.05$, and $|\varepsilon| = 6$; (a) and (b) are plotted in different windows of x and y .

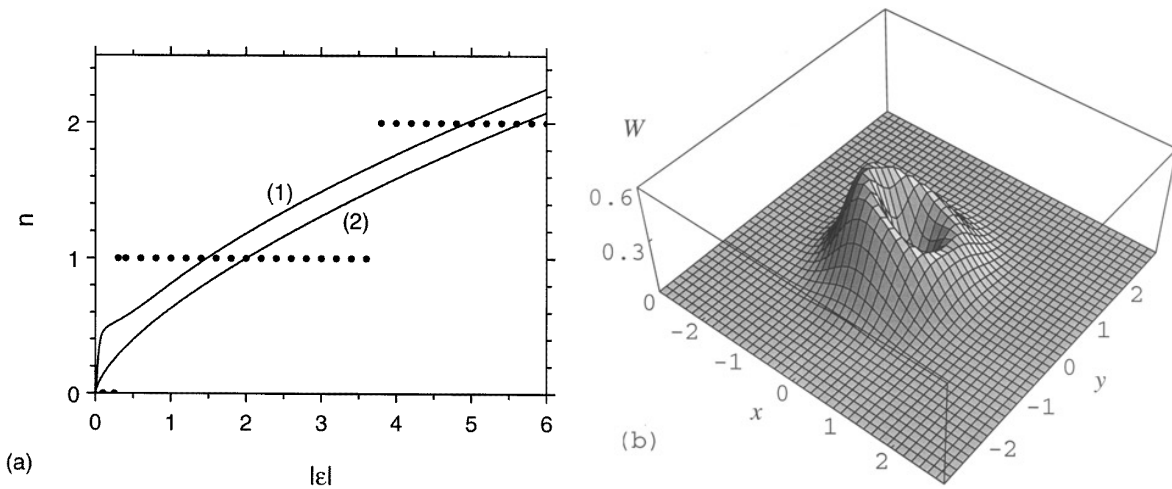


Figure 6. The same as in figure 1 (in (a) curves (1) and (2) correspond to quantum mechanical and semiclassical intensities, respectively) but for $\Delta/\chi'' = 0$ and $\gamma/\chi'' = 0.05$; (b) the corresponding Wigner function for $|\varepsilon| = 3$.

$$|\varepsilon| = |E|/\sqrt{(\chi')^2 + (\chi'')^2}. \quad (20)$$

Therefore the above discussion and examples, given for specific values of $\text{Re } \lambda = \Delta/\chi''$, $\text{Im } \lambda = -\gamma/\chi''$, and $|\varepsilon| = |E|/|\chi''|$, can equally be viewed as describing the cases with nonzero χ' , as long as the parameters γ , Δ , χ' , χ'' , and $|E|$ result in the same values of $\text{Re } \lambda$, $\text{Im } \lambda$, and $|\varepsilon|$, as defined by equations (18)–(20). For example, the graphs of figure 3, where $\text{Re } \lambda \equiv a = -0.5$ and $\text{Im } \lambda \equiv b = -10^{-5}$, can be viewed as representing the case with nonzero χ' and χ'' if we choose $\Delta = a\chi'' + b\chi'$ and $\gamma = a\chi' - b\chi''$. Obviously, there are additional limitations to be included in the consideration, such as the requirement that the cavity damping constant γ should remain positive valued. In the above example ($a = -0.5$, $b = -10^{-5}$) this may require rather large values of χ'' , or the magnitude of the two-photon absorption rate χ' must be limited, so that $\chi''/\chi' > a/b$.

More generally, the interplay between the χ' and χ'' effects can easily be established by considering the behaviour of the system in terms of the semiclassical steady states and bistability regions. Following [11] these can be found to be

given by the following state equation:

$$|\varepsilon| = 4n^3 + 4(\text{Re } \lambda)n^2 + |\lambda|^2 n, \quad (21)$$

with turning points

$$n^\pm = \left[-2(\text{Re } \lambda) \pm \sqrt{4(\text{Re } \lambda)^2 - 3|\lambda|^2} \right] / 6. \quad (22)$$

These results generalize equations (2.18) and (2.19) of [11] to the case of nonzero χ' (or arbitrary values of the complex parameter $\chi = \chi' + i\chi''$). Correspondingly, the bistability requires now that $\text{Re } \lambda \propto \gamma\chi' + \Delta\chi'' < 0$, and $(\text{Re } \lambda)^2 > 3(\text{Im } \lambda)^2$. It is easily seen now that if the cavity is only filled by a two-photon absorber (i.e. $\chi'' = 0$, and $\chi = \chi'$) then we obtain $\text{Re } \lambda = \gamma/\chi' > 0$, and therefore the bistability (as well as the examples of figures 1–4, where $\text{Re } \lambda < 0$) cannot be realized.

In the general case of both χ' and χ'' being nonzero, the overall influence of the two-photon absorption mechanism is that it reduces the bistability region, leading the system towards the monostable (in the limit of large χ') behaviour. Alternatively speaking, when including the two-photon losses, to guarantee the observation of the effects

characteristic for a manifestly bistable regime, one would need to employ χ'' values and cavity detunings Δ of opposite signs and of larger absolute values.

4. Summary

In summary, we have presented an exact Wigner-function solution to the model of a driven anharmonic oscillator, in the steady state regime. This allowed us to explicitly visualize the phase-space images of the state of the cavity mode, which demonstrate, in particular, a rich variety of transition scenarios from the low to higher level of photon excitation. An analysis of the system in terms of the photon number probability distribution has been provided as well.

Of particular interest is the behaviour of the system in the extreme quantum regime (corresponding to strong nonlinearities or low damping), where intuitive predictions are likely to fail. The results in this regime show qualitative departure of the steady state of the cavity mode from behaviour in the semiclassical regime, thus making meaningless such conventional attributes of the model as bistability or turning points. In addition, while the dissipation washes out as, usually, quantum superposition and interference effects, nevertheless their contribution in the resulting Wigner function can still be clearly tracked via the obtained analytic form of the solution.

Acknowledgment

The author gratefully acknowledges P D Drummond for valuable discussions and for bringing [24] to his attention.

References

- [1] Hillery M, O'Connell R F, Scully M O and Wigner E P 1984 *Phys. Rep.* **106** 121
- [2] Bužek V and Knight P L 1995 *Progress in Optics* vol XXXIV, ed E Wolf (Amsterdam: North-Holland)
- [3] Vogel K and Risken H 1989 *Phys. Rev. A* **40** 2847
See also Leonhardt U 1997 *Measuring the Quantum State of Light* (Cambridge: Cambridge University Press)
- [4] Smithey D T, Beck M, Raymer M O and Faridani A 1993 *Phys. Rev. Lett.* **70** 1244
- [5] Breitenbach G, Muller T, Pereira S F, Poizat J-Ph, Schiller S and Mlynek J 1995 *J. Opt. Soc. Am. B* **12** 2304
Breitenbach G, Schiller S and Mlynek J 1997 *Nature* **387** 471
- [6] Kinsler P and Drummond P D 1991 *Phys. Rev. A* **43** 6194
- [7] Reid M D and Yurke B 1992 *Phys. Rev. A* **46** 4131
- [8] Kheruntsyan K V, Krähmer D S, Kryuchkyan G Yu and Petrossian K G 1997 *Opt. Commun.* **139** 157
- [9] Banaszek K and Knight P L 1997 *Phys. Rev. A* **55** 2368
Felbinger T, Schiller S and Mlynek J 1998 *Phys. Rev. Lett.* **80** 492
- [10] Hug M, Menke C and Schleich W 1998 *Phys. Rev. A* **57** 3188
Hug M, Menke C and Schleich W 1998 *Phys. Rev. A* **57** 3206
- [11] Drummond P D and Walls D F 1980 *J. Phys. A: Math. Gen.* **13** 725
- [12] Collett M J and Walls D F 1985 *Phys. Rev. A* **32** 2887
- [13] Milburn G J 1986 *Phys. Rev. A* **33** 674
- [14] Milburn G J and Holmes C A 1986 *Phys. Rev. Lett.* **56** 2237
- [15] Yurke B and Stoller D 1986 *Phys. Rev. Lett.* **57** 13
- [16] Kitagawa M and Yamamoto Y 1986 *Phys. Rev. A* **34** 3974
Yamamoto Y, Machida S, Imoto N, Kitagawa M and Björk G 1987 *J. Opt. Soc. Am. B* **4** 1645
- [17] Daniel D J and Milburn G J 1989 *Phys. Rev. A* **39** 4628
- [18] Parkins A S and Walls D F The physics of trapped dilute-gas Bose–Einstein condensates, at press
- [19] Chaturvedi S, Drummond P D and Walls D F 1977 *J. Phys. A: Math. Gen.* **10** L187
- [20] Louisell W H 1973 *Quantum Statistical Theory of Radiation* (New York: Wiley)
- [21] Gardiner C W 1986 *Handbook of Stochastic Methods* (Berlin: Springer)
- [22] Erdélyi A (ed) 1953 *Higher Transcendental Functions (Bateman Manuscript Project)* vol 1 (New York: McGraw-Hill)
- [23] Erdélyi A (ed) 1953 *Higher Transcendental Functions (Bateman Manuscript Project)* vol 2 (New York: McGraw-Hill)
- [24] Imamoglu A, Schmidt H, Woods G and Deutsch M 1997 *Phys. Rev. Lett.* **79** 1467
- [25] Gilles L, Garraway B M and Knight P L 1994 *Phys. Rev. A* **49** 2785